Detection of diffusion anisotropy due to particle asymmetry from single-particle tracking of Brownian motion by the large-deviation principle

Itsuo Hanasaki* and Yoshitada Isono
Department of Mechanical Engineering, Graduate School of Engineering, Kobe University, 1-1 Rokkodai-cho, Nada-ku, Kobe 657-8501, Japan
(Received 7 March 2012; published 25 May 2012)

We show that the diffusion anisotropy due to the asymmetry of the particle can be extracted from the trajectory data without the information of the particle orientation. The subject of analysis is typical in single-particle tracking (SPT) experiments, and the analysis is based on the large-deviation principle in mathematics. We consider the model system of Langevin equations in two dimensions where a particle diffusion shows anisotropy depending on a single parameter defined by the two diffusion coefficients in the perpendicular directions of the frame fixed to the particle. We show how the large-deviation quantities depend on this parameter so that it can be used for the detection of the diffusion anisotropy. We also illustrate how the discreteness of the sampling interval in the SPT and the finiteness of the number of samples influence the results of the analysis.

DOI: 10.1103/PhysRevE.85.051134 PACS number(s): 05.40.−a

I. INTRODUCTION

The diffusion characteristics of anisotropic Brownian particles have been attracting much attention [1–12]. The applications include the self-organization and assembly mechanism of liquid crystals or solids observed in the solution of nanorods [13–16] partly because the fabrication of crystal structures from nanorods is directly related to the development of novel electronic devices and metamaterials [17,18]. Although some aspects of the design principle are suggested [18], there are various factors that affect the structure in specific situations [19–22]. In the first place, the assembly of nanorods accompanies the complexity due to its anisotropy, in contrast to the spherical nanoparticles. A straightforward solution to determine the assembly mechanism is the direct observation and detailed analysis of the elementary process. In fact, there have been drastic improvements in the visualization technique of diffusing small agents, which is often called single-particle tracking (SPT) [23–45]. This innovation offers the opportunity to extract particle trajectories at finer spatiotemporal resolutions for longer periods of time than before. However, the particle orientation is not always directly observable, especially when tracking the motion of single molecules by the light emitted from the attached marker molecules. There are a few techniques to observe the molecular orientation [37,46], but they are not widespread.

On the other hand, the understanding of raw data obtained from the experimental systems is still not sufficient. The basic quantity to characterize diffusion is the mean square displacement (MSD) derived from the particle trajectory. The diffusion coefficient can be obtained from the MSD when it is a linear function of time, but the available information is limited as long as the analysis relies on the MSD alone. Diffusion of asymmetric particles such as ellipsoids and rods is characterized by their anisotropic diffusion coefficients in the longitudinal and its perpendicular direction as well as the rotational diffusion coefficient. The motion of rods and ellipsoids appears the same as isotropic particles if we only observe the long-time limit of the diffusive behavior by the MSD. The MSD does not depend on the anisotropy and it is just linear if the marker of the particle is located at the center of diffusion. Therefore, it is not enough to observe only MSD if a deeper understanding is necessary. There is still room for innovation by theoretical analysis of the obtained data even when the experimental system setup is fixed. Although there has been a report to propose a function to deduce the anisotropy of the diffusing particle from the SPT data [47], the development of a theoretical approach for the SPT is still lacking compared to the hardware developments. It is desirable for the multiple approaches in the analysis to be implemented because different factors inherent to the system can lead to the same observable feature when the difference between the theoretical model and the experimental system is not clear enough. This can often be the case when the subject is biological, and this is similar to the situation in which a diagnosis is made from symptoms. It might also become possible to distinguish between the external noise and the inherent fluctuating signal of the diffusion depending on the source of noise.

In this article, we show that the information of diffusion anisotropy can be elucidated from the particle trajectory data where the particle is defined just as a single point indicating only the position at every time step of observation. We use the large-deviation principle of statistics. Although it has been pointed out that the large-deviation principle is effective for extracting the non-Gaussian characteristics of diffusive dynamics [48,49], these studies focused on the illustration of analytically solvable models such as random walk on a one-dimensional lattice [48], or the peculiarity of the order-parameter dependence on the deterministic diffusion generated from a chaotic map [49]. We focus on the anisotropy of Brownian motion, which is ubiquitous and important in a vast range of applications from material science and device physics to biology and medicine. We show how the diffusion anisotropy is reflected in the quantities related to the large-deviation principle. We consider the simple model system to obtain the trajectory data corresponding to what is

*hanasaki@mech.kobe-u.ac.jp

available through SPT experiments, and we also discuss how the numerical treatment affects the large-deviation analysis of the experimental systems.

II. MODEL AND METHODS

A. Two-dimensional anisotropic Brownian diffusion

We consider a model system of two-dimensional diffusion by a single anisotropic particle. This two-dimensionality is the typical situation of SPT experiments. We define the anisotropic Brownian motion by three parameters: the rotational diffusion coefficient D_r and the translational diffusion coefficients D_a,D_b in two directions, where $D_\mathrm{a} \geqslant D_\mathrm{b}$. D_a and D_b correspond to the diffusion coefficients in the longitudinal and its perpendicular directions when the particle of interest is a rod, ellipsoid, or a kind of prolate particle. However, the anisotropy in the diffusion of smaller objects such as biomolecules might not be interpreted as being caused only by the geometric anisotropy in a macroscopic notion but by the hydrophilic-hydrophobic balance or generally the charge distribution in it. The origin of diffusion anisotropy in this model system is solely due to $D_\mathrm{a}/D_\mathrm{b} > 1$, which does not limit the origin of diffusion anisotropy to specific factors.

We assume that the Brownian motion in each translational direction and rotational motion is generated from the Wiener process. Then, the Brownian dynamics of the anisotropic diffusion can be described as follows [2,5,11,47]:

$$\frac{d}{dt}\begin{bmatrix} x(t) \\ y(t) \end{bmatrix} = \begin{bmatrix} \sqrt{2D_\mathrm{a}}\cos^2\theta(t) + \sqrt{2D_\mathrm{b}}\sin^2\theta(t) & (\sqrt{2D_\mathrm{a}} - \sqrt{2D_\mathrm{b}})\cos\theta(t)\sin\theta(t) \\ (\sqrt{2D_\mathrm{a}} - \sqrt{2D_\mathrm{b}})\cos\theta(t)\sin\theta(t) & \sqrt{2D_\mathrm{a}}\sin^2\theta(t) + \sqrt{2D_\mathrm{b}}\cos^2\theta(t) \end{bmatrix}\begin{bmatrix} \xi_x(t) \\ \xi_y(t) \end{bmatrix}, \tag{1}$$

$$\frac{d\theta(t)}{dt} = \sqrt{2D_\mathrm{r}}\xi_\theta(t), \tag{2}$$

where $(x(t), y(t))$ is the position of the center of diffusion and $\theta(t)$ is the orientation of the particle; ξ_x, ξ_y, and ξ_θ are the Gaussian random variables that satisfy the mean 0, variance 1, and $\langle \xi_i(t)\xi_i(t')\rangle = \delta(t-t')$, where $i = x$, y, and θ; and $\langle\,\rangle$ stands for the ensemble average. The use of $x(t)$ and $y(t)$ defined in this way in the analysis means that we consider the situations in which the distance of the marker position in the particle of interest from its center of diffusion is negligible. Defining the characteristic length L, time τ, and anisotropy parameter η by

$$L = \left(\frac{D_\mathrm{a} + D_\mathrm{b}}{2D_\mathrm{r}}\right)^{\frac{1}{2}}, \tag{3}$$

$$\tau = D_\mathrm{r}^{-1}, \tag{4}$$

$$\eta = \frac{D_\mathrm{a} - D_\mathrm{b}}{D_\mathrm{a} + D_\mathrm{b}}, \tag{5}$$

the Langevin Eqs. (1) and (2) can be nondimensionalized as

$$\frac{d\boldsymbol{X}}{dt} = \left[\sqrt{2}(1+\eta)^{\frac{1}{2}}\hat{\boldsymbol{u}}\hat{\boldsymbol{u}} + \sqrt{2}(1-\eta)^{\frac{1}{2}}(\boldsymbol{I} - \hat{\boldsymbol{u}}\hat{\boldsymbol{u}})\right]\cdot\boldsymbol{\Xi}(t), \tag{6}$$

$$\frac{d\theta}{dt} = \sqrt{2}\xi_\theta(t), \tag{7}$$

where $\boldsymbol{X} = (x,y)^T$, $\boldsymbol{\Xi} = (\xi_x,\xi_y)^T$, $\hat{\boldsymbol{u}} = (\cos\theta(t), \sin\theta(t))^T$, and I is the two-dimensional unit matrix [47]. We solve the above equations numerically by the following rules:

$$\theta(t+\Delta t) = \theta(t) + \sqrt{2\Delta t}\xi_\theta(t), \tag{8}$$

$$\boldsymbol{X}(t+\Delta t) = \boldsymbol{X}(t) + \frac{\sqrt{\Delta t}}{2}[\boldsymbol{F}(t+\Delta t) + \boldsymbol{F}(t)]\cdot\boldsymbol{\Xi}(t), \tag{9}$$

$$\boldsymbol{F}(t) = \sqrt{2}(1+\eta)^{\frac{1}{2}}\hat{\boldsymbol{u}}(t)\hat{\boldsymbol{u}}(t) + \sqrt{2}(1-\eta)^{\frac{1}{2}}[\boldsymbol{I} - \hat{\boldsymbol{u}}(t)\hat{\boldsymbol{u}}(t)], \tag{10}$$

where Δt is the time step in the numerical integration [47]. The parameter Δt corresponds to the frame rate of the video capture in the SPT experiments. Nondimensionalized quantities are used, and the characteristic time scale (and correspondingly the rotational diffusion coefficient) is fixed to be $\tau = 1$ throughout this article. Thus, the only tunable parameter in the physical property of the dynamics is η. On the other hand, the standard condition for the total duration of the simulation is defined to be $n_\mathrm{tot} = 10^6$ time steps with $\Delta t = 10^{-2}$, but the influence of these parameters is examined later.

B. Calculation of large-deviation quantities

The non-Gaussian nature of a fluctuating quantity $U(t)$ in a steady state can be analyzed on the basis of the large-deviation principle [48,49]. In contrast to the fact that the central limit theorem provides the Gaussian nature of an independent and identically distributed stochastic variable by focusing on the sample mean in the long-time limit, the large-deviation analysis first considers the finite-time mean,

$$\bar{u}(T) = \frac{1}{T}\int_t^{t+T} U(s)ds, \tag{11}$$

where T is the time span to take the mean value. The finite-time mean $\bar{u}(T)$ is then used for the calculation of a characteristic function $\phi(q)$ by

$$\phi(q) = \lim_{T\to\infty}\frac{1}{T}\ln\langle\exp[qT\bar{u}(T)]\rangle, \tag{12}$$

where q is a real-number parameter. $\phi(q)$ is also called the scaled cumulant-generating function [50]. In the large-deviation theory, $\phi(q)$ can be related to the rate function defined by

$$S(u) = -\lim_{T\to\infty}\frac{1}{T}\ln P(\bar{u}\in[u,u+du]) \tag{13}$$

through the Gärtner-Ellis theorem as

$$S(u(q)) = \sup_q [qu(q) - \phi(q)], \tag{14}$$

where $P(\bar{u} \in [u, u+du])$ is the probability that $\bar{u}$ takes the value between u and $u+du$. The rate function indicates the speed of convergence to the most probable value. Equation (14) reduces to

$$S(u(q)) = qu(q) - \phi(q) \tag{15}$$

when $\phi(q)$ is strictly convex and differentiable. $u(q)$ is obtained by the derivative of Eq. (15) with respect to q:

$$u(q) = \frac{d\phi(q)}{dq}. \tag{16}$$

In Ref. [49], the quantity

$$\chi(q) = \frac{du(q)}{dq} = \frac{d^2\phi(q)}{dq^2} \tag{17}$$

was also introduced as the susceptibility.

In this study, we calculate the large-deviation quantities numerically from the time-series data of particle trajectory. Therefore, we cannot take $T \to \infty$ but use the finite number of time steps $n_{\rm span}$ which corresponds to T by $T = n_{\rm span}\Delta t$. Similarly, we cannot take the infinite number of samples for the ensemble average $\langle\ \rangle$ in Eq. (12), but we use a finite number of samples $n_{\rm ens}$ which is determined by the available amount of data, and the maximum is $n_{\rm ens} = n_{\rm total}/n_{\rm span}$. Therefore, the maximum $n_{\rm span}$ and $n_{\rm ens}$ are not independent of each other.

III. RESULTS AND DISCUSSION

Figure 1 shows the trajectories of the diffusion defined by Eqs. (6) and (7) with different anisotropy parameters ($\eta = 0$, 0.5, and 1), and time steps ($\Delta t = 10^{-3}$ and 10^{-2}). The cases of $\eta = 0$ [Figs. 1(a) and 1(b)] correspond to the isotropic diffusion ($D_{\rm a} = D_{\rm b}$), and $\eta = 1$ [Figs. 1(e) and 1(f)] corresponds to the case when $D_{\rm b}$ is negligible compared to $D_{\rm a}$. The difference in the anisotropy parameter $\eta = 0$ and 1 can be easily recognized for both cases of the time steps, and the anisotropy is more pronounced for smaller time steps [Fig. 1(e) compared to Fig. 1(f)] under the condition of the same number of total time steps. More intuitively, the displacement in the x direction tends to be larger when the rod is directed in the x direction while it is smaller when it is directed in the perpendicular (i.e., y) direction if the diffusing particle is a rod. However, such a distinction by visual inspection is qualitative, and Figs. 1(c) and 1(d) show that even a qualitative distinction is difficult when η is not far enough from 0. The difference between $\eta = 0.5$ and 0 is difficult to recognize directly from these samples even for the smaller time step $\Delta t = 10^{-3}$. The time steps much smaller than $\Delta t = 10^{-3}$ may improve the ease of distinction, but the time step is not an arbitrary parameter. In reality, e.g., in the case of SPT experiments, the smallest time step is limited by the specification of the video capturing system. In addition, the smaller time steps for the same duration of observation time mean a larger amount of total data storage. In general, the total amount of time required for the observation of the phenomena of interest is not always known *a priori*. Thus, the time step cannot be arbitrarily small while desired in general. We show the influence of time-step scale on the results of the analysis later.

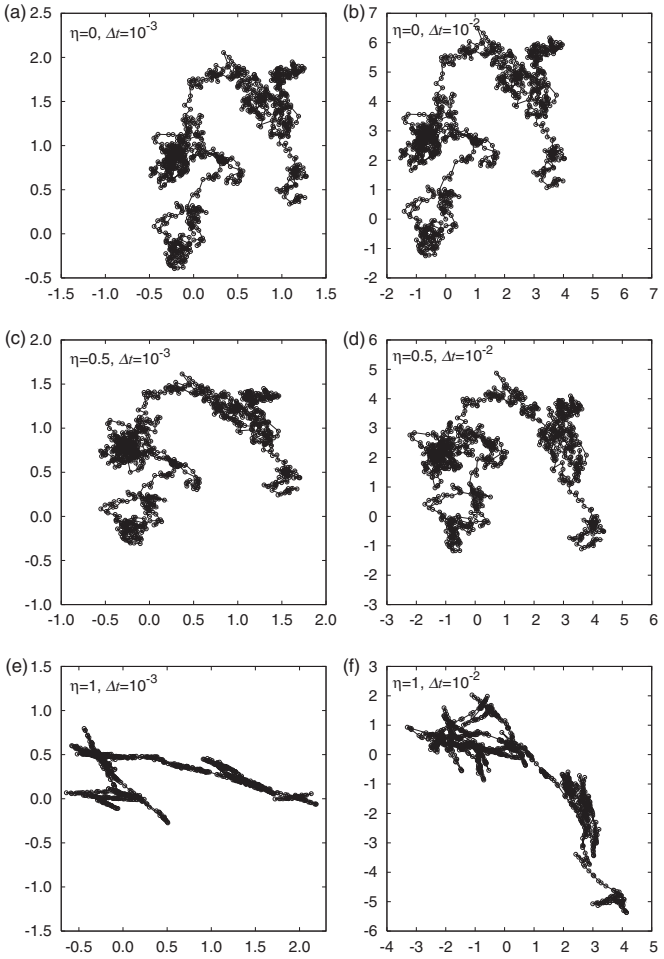

FIG. 1. Sample trajectories of Brownian motion under different conditions of anisotropy parameter η defined in Eq. (5) and time step Δt. All the trajectories have been generated from the same random number sequences following the rule defined in Eqs. (6) and (7) with $\tau = 1$. The total number of time steps shown is fixed to be 10^3, and hence the corresponding time duration changes accordingly.

The typical quantity for the analysis of diffusion is the MSD, but the MSD is independent of anisotropy parameter η [47]. The linear MSD with different magnitude of slope cannot quantify the diffusion anisotropy, and it merely indicates the overall isotropic diffusivity corresponding to the overall diffusion coefficient. However, the large-deviation quantities reveal this anisotropy. Figure 2 shows the large-deviation quantities $\phi_{\rm m}(q)$, $u_{\rm m}(q)$, $\chi_{\rm m}(q)$, and $S_{\rm m}(u_{\rm m})$ defined as follows:

$$\phi_{\rm m}(q) = \tfrac{1}{2}[\phi_x(q) + \phi_y(q)], \tag{18}$$

$$u_{\rm m}(q) = \tfrac{1}{2}[u_x(q) + u_y(q)], \tag{19}$$

$$\chi_{\rm m}(q) = \tfrac{1}{2}[\chi_x(q) + \chi_y(q)], \tag{20}$$

$$S_{\rm m}(u_{\rm m}) = \tfrac{1}{2}[S_x(q) + S_y(q)], \tag{21}$$

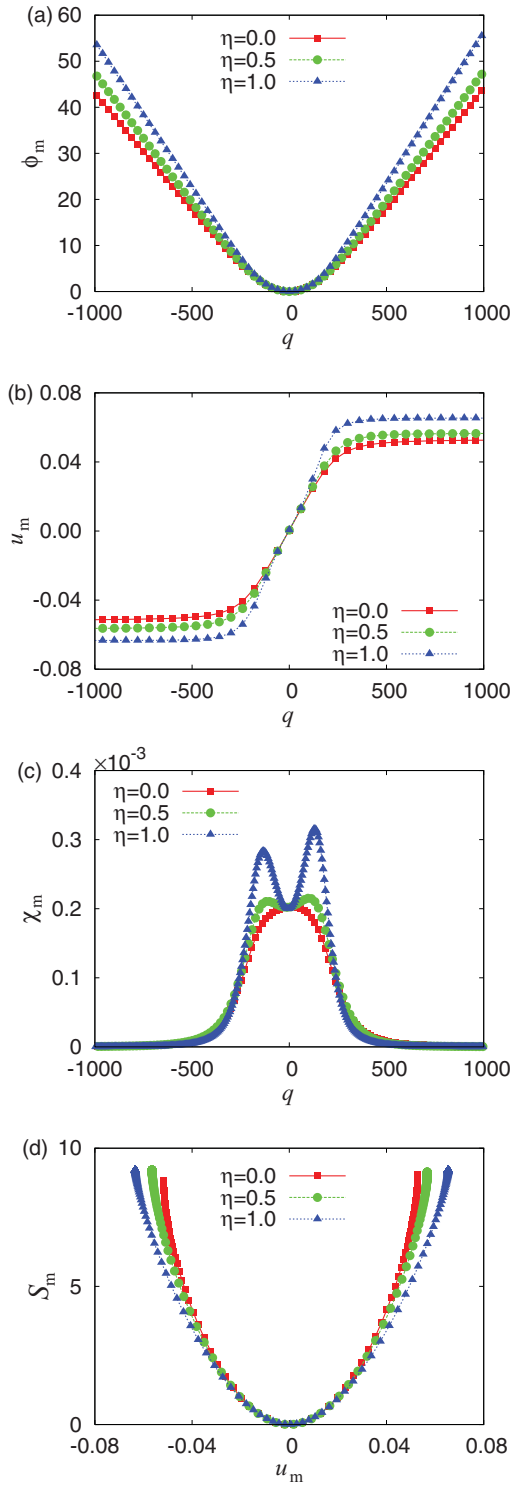

FIG. 2. (Color online) Large-deviation quantities obtained from the displacement per time step under different conditions of anisotropy parameter η with $\Delta t = 10^{-2}$, $n_{\rm tot} = 10^6$, and $T = 1$: (a) $\phi_{\rm m}(q)$, (b) $u_{\rm m}(q)$, (c) $\chi_{\rm m}(q)$, and (d) $S_{\rm m}(u_{\rm m})$.

where the subscripts x and y stand for the large-deviation quantities derived from the displacements per time step in the x and y directions in an arbitrary laboratory frame. In the definition of Eq. (21), an independent variable $u_{\rm m}$ is related to each point of value of $S_{\rm m}$ by the same values of q as those correspond to the right-hand side of Eq. (21). The x and y directions in the laboratory frame do not require the information of the particle orientation. The x and y directions are equivalent in a sense that the infinite number of samples will yield the same values of large-deviation quantities, and the difference originates from the finiteness of the number of samples. Thus, Eqs. (18)–(21) are defined to make full use of the experimentally obtained data. In the numerical calculation of Eq. (12), the following definition of $\bar{u}$ is used in place of Eq. (11):

$$\bar{u}(n_{\rm span}) = \frac{1}{n_{\rm span}} \sum_{i=1}^{n_{\rm span}} U(i), \tag{22}$$

where $U(i)$ stands for the displacement per time step at the ith step. Figure 2 was obtained under the conditions of $\Delta t = 10^{-2}$ and total time of 10^4 (i.e., $n_{\rm tot} = 10^6$ steps), and $T = 1$ (i.e., $n_{\rm span} = 10^2$). That is, we split the number sequences of 10^6 steps into 10^4 sets of data, each consisting of 10^2 numbers. If we take longer T, we have fewer samples $n_{\rm ens}$ for the ensemble average $\langle\,\rangle$ in Eq. (12). We examine the influence of this choice on the result of the analysis later.

It can be seen from Fig. 2(a) that the slope of the scaled cumulant-generating function $\phi_{\rm m}(q)$ for large q depends on the anisotropy η. This trend is more straightforwardly illustrated by $u_{\rm m}(q)$ [Fig. 2(b)], i.e., the derivative of $\phi_{\rm m}(q)$ with respect to q. The asymptotic values exist for both $q \to \pm\infty$, and $u_{\rm m}(\infty)$ is larger for higher anisotropy. The absolute value of $u_{\rm m}(-\infty)$ is also larger for higher anisotropy. This is due to the fact that the distribution of $\bar{u}$ is symmetric in a sense that the positive and negative values with the same absolute values have the same probability of occurrence. Namely, there is no asymmetry in the definition of positive and negative directions of displacements. Hence, $u_{\rm m}(\infty) = -u_{\rm m}(-\infty)$ for the long-time limit. The difference of $u_{\rm m}(\pm\infty)$ due to η can be used for the signal to detect the diffusion anisotropy. Although the difference of $\phi_{\rm m}(q)$ and $u_{\rm m}(q)$ in the vicinity of $q = 0$ is not clear, $\chi_{\rm m}(q)$ is remarkably different [Fig. 2(c)]. $\chi_{\rm m}(q)$ is unimodal when the diffusion is completely isotropic ($\eta = 0$). On the other hand, when the particle motion is anisotropic ($\eta > 0$), the bimodal distribution emerges. The generalized variance $\chi_{\rm m}(q)$ at $q = 0$ has one-to-one correspondence to the diffusion coefficient, and the value does not change with η. The ordinary diffusion coefficient does not provide information of the diffusion anisotropy as already mentioned. On the other hand, the nonzero q reveals the difference of $\chi_{\rm m}(q)$ originating from the difference of η.

The η dependence of the rate function $S_{\rm m}(u_{\rm m})$ is also observed [Fig. 2(d)]. The rate function does not show a noticeable difference in the regime of small deviation from $u = 0$, but the diffusion anisotropy is reflected in the regime of large deviation. The values of $S_{\rm m}(u_{\rm m})$ with the same $u_{\rm m}$ are largest at $\eta = 0$ and smallest at $\eta = 1$. Considering the basic fact that the rate function indicates the speed (or the necessary length of numerical sequence) of convergence to the mean value, this difference means that the displacement per time step converges more slowly for anisotropic diffusion than for isotropic diffusion, where the latter is defined by the single value of the diffusion coefficient. If the particle diffusion is anisotropic, it has two distinctive diffusion coefficients. This

leads to a broader range of occurrence in the displacement per step. The rate function S_G of the sample mean of Gaussian distribution obeys $S_G(u) = (u - \mu_G)^2/(2\sigma_G^2)$ [50], where μ_G and σ_G are the mean value and the standard deviation, respectively. The $S_G(u)$ at specific values of u takes smaller values for the dynamics with larger σ_G. If the dynamics is intrinsically purely Gaussian, then the difference in the variance is reflected in the MSD, or equivalently the diffusion coefficient. However, the system of interest here is the nondimensionalized equations (3)–(7), and the difference in the dynamics originates only from diffusion anisotropy η. Nevertheless, the existence of two distinctive diffusion coefficients leads to the smaller value of the rate function $S_m(u)$. Thus, all of the large-deviation quantities $\phi_m(q)$, $u_m(q)$, $\chi_m(q)$, and $S_m(u_m)$ reflect the difference of anisotropy η. In addition, the difference between $\eta = 0$ and 0.5 can be observed, whereas it was not clear from the visual inspection of the trajectories themselves (Fig. 1). The most sensitive of the four quantities is apparently $\chi_m(q)$. However, the two peaks in the case of $\eta = 1$ show some asymmetry with respect to the positive and negative side of q, which is basically caused by the finiteness of the number of samples. Therefore, it is safer to analyze all of these large-deviation quantities in order to confirm that the observed difference is significant.

Since the diffusive phenomenon is observed in various fields from physics to biology to engineering in a broad sense, the characteristic time scales of the potential applications have a broad range. Although the SPT of biomolecules in a fluidic medium may sometimes demand a higher time resolution than is possible today, the diffusion in a solid may consist of rare events of hopping between the available sites as an elementary process. In fact, the biomolecules in a cell membrane exhibit hopping events from one compartment to another [27]. These cases might require a huge amount of data storage, and then the choice of the observation time step becomes the important decision. Such choices should be based on the already available knowledge on the subject of observation, but it is also necessary to know the basic influence of the time step on the large-deviation quantities obtained from the finite number of samples.

Figure 3 shows the large-deviation quantities for $\eta = 0.5$ and $n_{span} = 10^2$ obtained under the different conditions of Δt. In order to see the direct influence of Δt, the total number of time steps is fixed to be 10^6 instead of the total duration of the dynamics. It can be observed that the difference in Δt leads to the differences in the large-deviation quantities, although the characteristic time scale τ is fixed. The larger Δt leads to larger values of $\phi_m(q)$ and the narrower range of the nonlinear part around $q = 0$. This obviously corresponds to the steeper $u_m(q)$ around $q = 0$ and the faster convergence to the larger asymptotic values. The larger Δt leads to the narrow range of nonzero $\chi_m(q)$ and the higher peaks. It becomes difficult to recognize the bimodality of $\chi_m(q)$ if Δt is too large. The $S_m(u_m)$ at specific values of $u_m(q)$ is smaller for larger Δt. The larger Δt means a longer time span of T with the same n_{span}, which leads to a higher possibility to explore the broader range of particle orientation θ and a different diffusivity in the specific direction in the coordinate of the laboratory frame. Thus, the large-deviation quantities

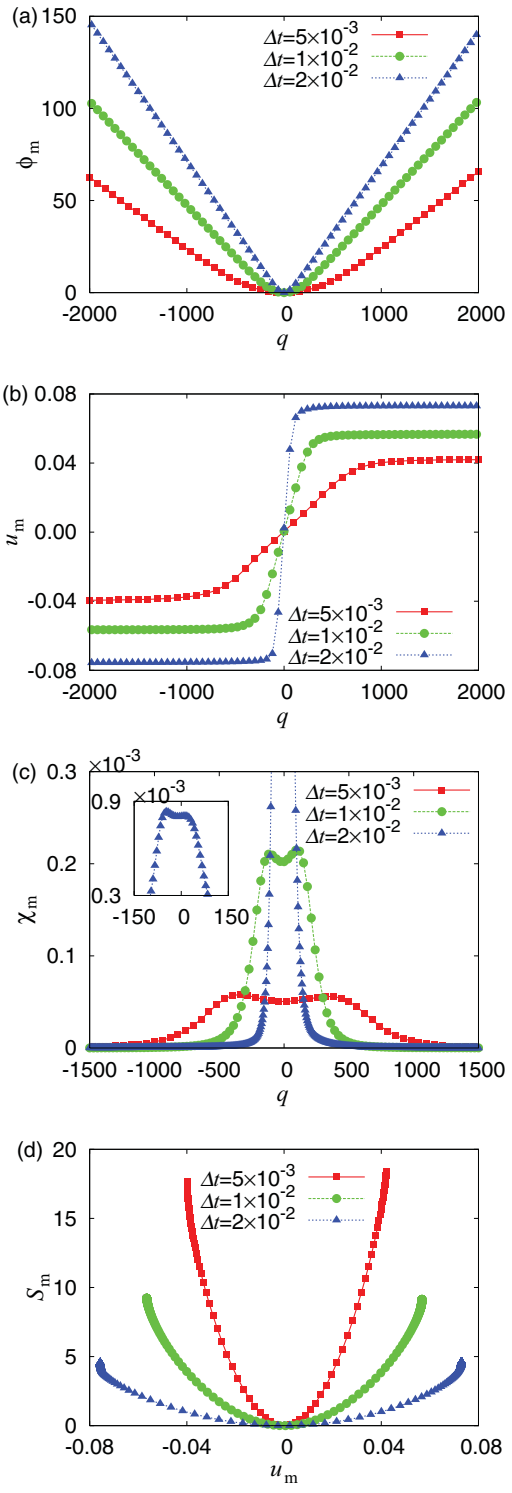

FIG. 3. (Color online) Large-deviation quantities obtained from the displacement per time step under different conditions of time step Δt with $\eta = 0.5$, $n_{span} = 10^2$, and $n_{tot} = 10^6$: (a) $\phi_m(q)$, (b) $u_m(q)$, (c) $\chi_m(q)$, and (d) $S_m(u_m)$. Note that the total time duration of the dynamics and T vary with Δt.

of different physical conditions have to be compared with the same Δt.

Although there are many influences on the large-deviation quantities, we focus on the Δt dependence of $u_m(\pm\infty)$ to

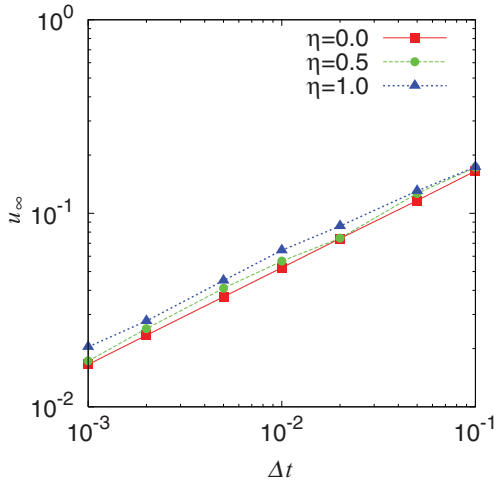

FIG. 4. (Color online) Δt dependence of u_∞ at $\eta = 0$, 0.5, and 1 with $n_{\rm span} = 10^2$ and $n_{\rm tot} = 10^6$. The total time duration of the dynamics and T are varied accordingly.

observe the trend quantitatively. Since $u_{\rm m}(\infty) = -u_{\rm m}(-\infty)$ due to the symmetry in the $\bar{u}(T)$ distribution, as we mentioned above, we define u_∞ as follows:

$$u_\infty = \tfrac{1}{2}[u_{\rm m}(\infty) - u_{\rm m}(-\infty)], \tag{23}$$

in order to make full use of the available finite set of data. The dependence of u_∞ on Δt is shown in Fig. 4. The u_∞ is smaller for smaller Δt, and the power-law relation is observed. The fitting to $u_\infty \propto \Delta t^\alpha$ indicates $\alpha = 0.499$, 0.496, and 0.470 for $\eta = 0.0$, 0.5, and 1.0, respectively. The trend of $u_\infty \propto \Delta t^{\frac{1}{2}}$ originates from the simple fact that the smaller time steps lead to smaller displacements per time step, which directly corresponds to the term of $\Delta t^{\frac{1}{2}}$ in Eq. (9). Figure 4 also exhibits a clear trend showing that u_∞ is larger for larger η. Furthermore, it can be confirmed in combination with the slope of the fitting that smaller Δt is advantageous for the distinction of η. This is consistent with the visual inspection of trajectories (Fig. 1) and with the consideration that the diffusion anisotropy should not be observable if $\Delta t \sim \tau$. If Δt is too large, even a short successive sequence of displacement per time step in a specific laboratory frame direction does not represent the diffusion coefficient defined at specific θ because the rotation of the particle of interest is too fast compared to the time step. The quantitative detail of the limit of acceptable Δt depends on the total number of sampled data as well as the external perturbative noise in the experiments.

Because the large-deviation theory itself deals with $T \to \infty$ in principle, it is important to examine the influence of finite T on the large-deviation quantities. Figure 5 shows the large-deviation quantities calculated under different conditions of T with $\eta = 0.5$ and $\Delta t = 10^{-2}$. $n_{\rm tot}$ is also fixed to be 10^6, which leads to different $n_{\rm ens}$ for different $n_{\rm span}$. Figure 5(a) indicates that larger T leads to smaller $\phi_{\rm m}(q)$. Correspondingly, $u_{\rm m}(\pm\infty)$ is smaller for larger T [Fig. 5(b)]. In contrast to the Δt dependence, the slope of $u_{\rm m}(q)$ around $q = 0$ does not change noticeably with T [Figs. 5(a) and 5(b)]. The q where $\chi_{\rm m}(q)$ takes the peak value is larger for smaller T, and a higher resolution of q is necessary for larger T to capture

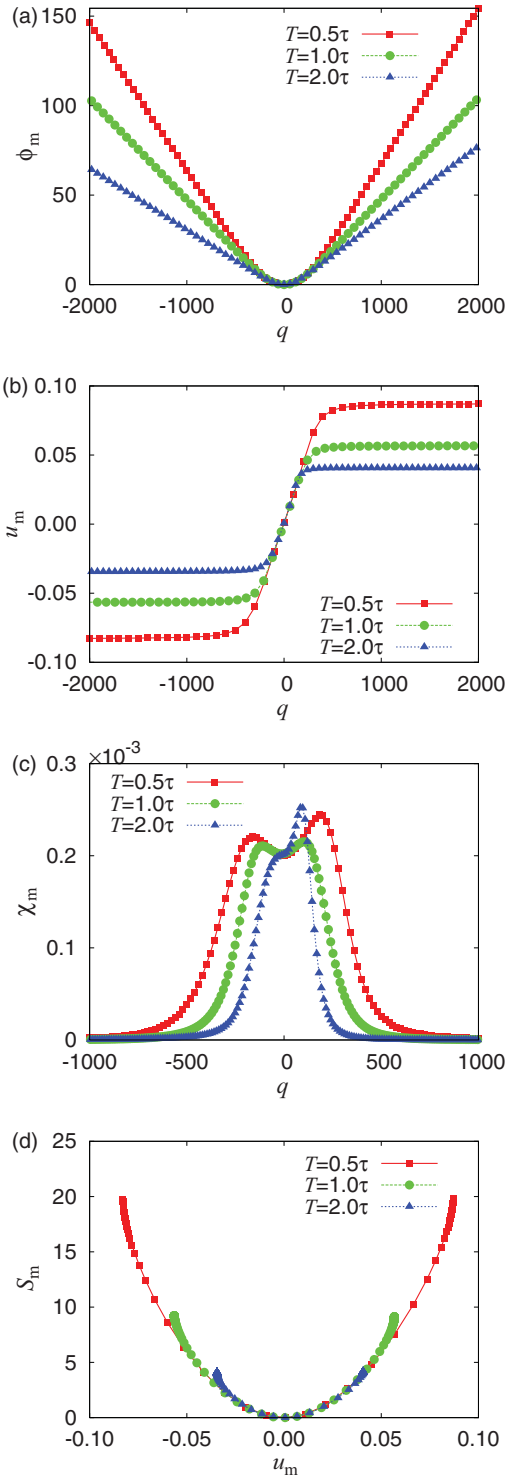

FIG. 5. (Color online) Large-deviation quantities obtained from the displacement per time step under different conditions of the span T with $\eta = 0.5$, $\Delta t = 10^{-2}$, and $n_{\rm tot} = 10^6$: (a) $\phi_{\rm m}(q)$, (b) $u_{\rm m}(q)$, (c) $\chi_{\rm m}(q)$, and (d) $S_{\rm m}(u_{\rm m})$. $n_{\rm ens}$ is varied accordingly.

the detail of $\chi_{\rm m}(q)$ at smaller q [Fig. 5(c)]. The bimodal nature of $\chi_{\rm m}(q)$ might be missed if the resolution of q is insufficient. The rate function $S_{\rm m}(u_{\rm m})$ shows a simple dependence on T [Fig. 5(d)]. The $S_{\rm m}$ does not vary significantly with T except for the noticeable deviation in the vicinity of $u_{\rm m}(\pm\infty)$. The choice

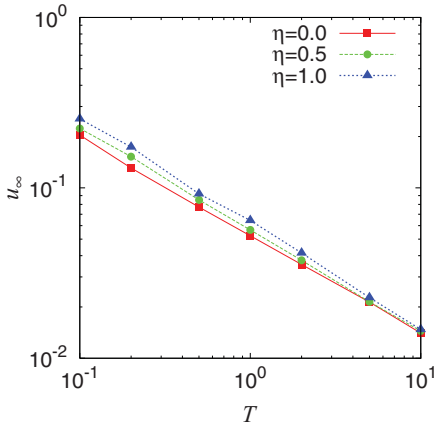

FIG. 6. (Color online) T dependence of u_∞ at $\eta = 0$, 0.5, and 1 with $\Delta t = 10^{-2}$ and $n_{\rm tot} = 10^6$. $n_{\rm ens}$ is varied accordingly.

of span T does not significantly alter the original essential large-deviation property exhibited by the rate function, but the larger T leads to a smaller range of $S_{\rm m}$ and $u_{\rm m}$. This property is caused by the basic nature of the large-deviation principle of this system, or rather the central limit theorem. Namely, the larger time span of the finite-time mean leads to a higher possibility of taking the values closer to the most probable value (i.e., 0 in this case).

The more quantitative relation between u_∞ and T is shown in Fig. 6. It should be noted that Fig. 6 is obtained under the condition of fixed $n_{\rm total}$. Therefore, $n_{\rm ens}$ is smaller for larger T. This corresponds to the situation in which a long time series of the raw data is obtained experimentally and the choice of T is flexible. Figure 6 shows the power-law behavior, and the larger η leads to larger u_∞. The fitting to $u_\infty \propto T^\gamma$ indicates $\gamma = -0.574$, -0.599, and -0.620 for $\eta = 0.0$, 0.5, and 1.0, respectively. Thus, the trend of a larger difference in u_∞ between the different η for smaller values of T is observed. The smaller T in this figure means larger $n_{\rm ens}$. The finiteness of not only T but also $n_{\rm ens}$ affects the overall property. In fact, the value of γ for $\eta = 0.0$ noticeably larger than $-1/2$ reflects the influence of variation in $n_{\rm ens}$. Figure 7 shows that u_∞ increases monotonically with $n_{\rm ens}$. When $n_{\rm ens}$ is fixed to be

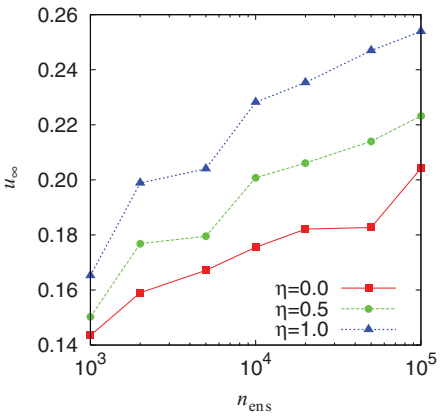

FIG. 7. (Color online) $n_{\rm ens}$ dependence of u_∞ at $\eta = 0$, 0.5, and 1 with $\Delta t = 10^{-2}$ and $n_{\rm span} = 10^1$. The total duration of the dynamics is varied accordingly.

10^3 (and $n_{\rm tot}$ is varied accordingly), the fitting to the power-law results is $\gamma = 0.503$, i.e., $u_\infty \propto T^{-\frac{1}{2}}$ when $\eta = 0$. This power law is essentially derived from the mechanism of the finite sample effect discussed in Ref. [51]. In our case, the threshold of observing the value around u (i.e., $[u,u+du]$) in $n_{\rm span}$ can be described as

$$n_{\rm span} \exp[-T S(u)] \propto 1 \tag{24}$$

from the large-deviation principle. If $S(u)$ is quadratic, i.e.,

$$S(u) = \tfrac{1}{2} S''(\mu_G)(u-\mu_G)^2, \tag{25}$$

substitution of $S(u)$ from Eqs. (24) to (25) yields the following expression:

$$u \propto \mu_G + \sqrt{\frac{2\ln n_{\rm span}}{S''}}\, T^{-\frac{1}{2}}. \tag{26}$$

This is also why $\gamma \neq -1/2$ when $\eta > 0$ and the difference of γ from $-1/2$ is larger for larger η. The non-Gaussian characteristics observed in the finite-time mean are pronounced for larger η.

As we have examined the influence of sampling discreteness and finiteness (from Δt and T) on the large-deviation quantities, now we would like to show the dependence of the large-deviation quantity on the diffusion anisotropy η in an explicit manner. As already shown in Fig. 2, the difference in η is reflected in the large-deviation quantities in many ways, namely the values of $\phi_{\rm m}(q)$, u_∞, the peak positions and bimodality of $\chi_{\rm m}(q)$, and $S(u)$ for u away from the mean value change with η. Here, we use u_∞ as the representative of these characteristics. In particular, we define the scaled u_∞ as follows:

$$u^*_\infty(\eta = a) = \frac{u_\infty(\eta = a)}{u_\infty(\eta = 0)} \tag{27}$$

because the absolute values of u_∞ vary with the choice of T. The dependence of u^*_∞ on η is shown in Fig. 8. The u^*_∞ increases monotonically with and depends roughly linearly on η except for some cases in the vicinity of $\eta = 0$ and 1. This

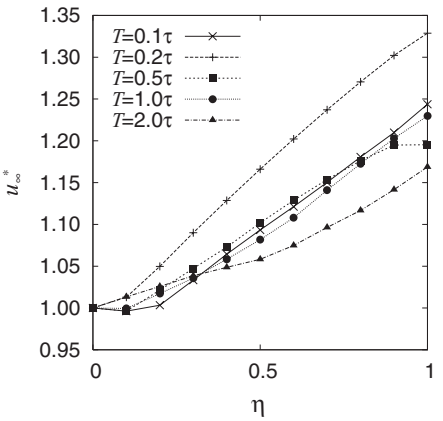

FIG. 8. Scaled u_∞ defined in Eq. (27) as a function of η under different conditions of T in combination with $n_{\rm ens}$ with $\Delta t = 10^{-2}$ and $n_{\rm tot} = 10^6$. All the trajectories with different conditions of η have been generated from the same random number sequences following the rule defined in Eqs. (6).

is useful for the comparison of η under different experimental conditions. On the other hand, the different combinations of T and n_{ens} lead to a substantial variation of $u^*_\infty(\eta)$ for the same raw data. Since the T dependence is not simply monotonic, this can be due to the finiteness of the number of samples. The absolute evaluation of η from a single scalar quantity by direct application of the large-deviation formalism in a straightforward manner will require a huge amount of raw data. Therefore, it is sensible to evaluate several large-deviation quantities in detail. There may be room for improvements in the numerical procedure as well, but it is beyond the scope of this article.

We used the finite-time mean Eq. (22) of the raw data instead of just estimating the rate function $S(u)$ by Eq. (13) from probability distribution. This is basically because we focused on several quantities related to the large-deviation principle rather than $S(u)$ alone. The probability distribution does not provide the information of time correlation, but the orientation of a prolate particle at a given instant depends on that of the past. Hence, the sequence of the fluctuation data with sufficiently small time step Δt holds the information of time correlation, which can be reflected in the finite-time mean. Although the large-deviation formalism is defined for $T \to \infty$, nonzero values of the finite sample mean are more frequently obtained for smaller T. Intuitively speaking, the observation of D_{a} relative to D_{b} is not the intermittent events if the rotation of the particle can be regarded as a Wiener process, and longer T is not likely to be advantageous for the distinction of η. On the other hand, it has been pointed out in Ref. [52] that the time span T has to be larger than the correlation time of the quantity for the finite-time mean in their case of the local expansion rate of the phase difference of the chaotic oscillator. In our case, at least the characteristic time scale is $\tau = D_\theta^{-1}$. However, the T dependence of $u_{\mathrm{m}}(\infty)$ is simply monotonic even in the range across $T = \tau$ (Fig. 6). This is attributed to the specific characteristics of the model system. Therefore, it is recommended that the dependence of T is examined in general applications where the dynamics of the system of interest is the target of the analysis.

IV. CONCLUDING REMARKS

In this study, we have shown that the large-deviation principle can be applied to compare the diffusion anisotropy by evaluating the trajectory data where the only available information is the particle position without orientation. The difference of diffusion anisotropy between different conditions of experiments can be compared without knowing the particle orientation at each time step as long as the precision, the resolution, and the amount of raw data are sufficient. When the particle is observed only via the marker position, it means that the distance between the center of diffusion for the particle of interest and the position of the marker attached to it is negligible. One has to be clear enough that the system under study is well-described by the presented model [i.e., Eqs. (1) and (2)] in the first place, because different factors can lead to the same symptoms as mentioned in the Introduction. When these conditions are satisfied, applications of the analysis presented here to SPT or particle image velocimetry experiments will offer highly valuable information that has not been appreciated until today.

ACKNOWLEDGMENTS

This work was supported by a Grant-in-Aid for Young Scientists (B), Japan.

[1] R. Vasanthi, S. Ravichandran, and B. Bagchi, J. Chem. Phys. **114**, 7989 (2001).
[2] T.-G. Tao, W. K. den Otter, J. T. Padding, J. K. G. Dhont, and W. J. Briels, J. Chem. Phys. **122**, 244903 (2005).
[3] Y. Han, A. M. Alsayed, M. Nobili, J. Z. T. C. Lubensky, and A. G. Yodh, Science **314**, 626 (2006).
[4] D. Mukhija and M. J. Solomon, J. Colloid Interface Sci. **314**, 98 (2007).
[5] R. Grima and S. N. Yaliraki, J. Chem. Phys. **127**, 084511 (2007).
[6] B. Bhaduri, A. Neild, and T. W. Ng, Appl. Phys. Lett. **92**, 084105 (2008).
[7] T. Munk, F. Höfling, E. Frey, and T. Franosch, Europhys. Lett. **85**, 30003 (2009).
[8] Y. Han, A. Alsayed, M. Nobili, and A. G. Yodh, Phys. Rev. E **80**, 011403 (2009).
[9] H. Zheng, S. A. Claridge, A. M. Minor, A. P. Alivisatos, and U. Dahmen, Nano Lett. **9**, 2460 (2009).
[10] J. T. Padding and W. J. Briels, J. Chem. Phys. **132**, 054511 (2010).
[11] A. Neild, J. T. Padding, L. Yu, B. Bhaduri, W. J. Briels, and T. W. Ng, Phys. Rev. E **82**, 041126 (2010).
[12] O. Güell, P. Tierno, and F. Gagués, Eur. Phys. J. Special Topics **187**, 15 (2010).
[13] L.-S. Li, J. Walda, L. Manna, and A. P. Alivisatos, Nano Lett. **2**, 557 (2002).
[14] D. V. Talapin, E. V. Shevchenko, C. B. Murray, A. Kornowski, S. Förster, and H. Weller, J. Am. Chem. Soc. **126**, 12984 (2004).
[15] S. Gupta, Q. Zhang, T. Emrick, and T. P. Russell, Nano Lett. **6**, 2066 (2006).
[16] J. L. Baker, A. Windmer-Cooper, M. F. Toney, P. L. Geissler, and A. P. Alivisatos, Nano Lett. **10**, 195 (2010).
[17] D. V. Talapin and C. B. Murray, Science **310**, 86 (2005).
[18] K. Stebe, E. Lewadndowski, and M. Ghosh, Science **325**, 159 (2009).
[19] D. J. Harris, H. Hu, J. C. Conrad, and J. A. Lewis, Phys. Rev. Lett. **98**, 148301 (2007).
[20] C. P. Lapointe, T. G. Mason, and I. I. Smalyukh, Science **326**, 1083 (2009).
[21] X. Ye, J. E. Collins, Y. Kang, J. Chen, D. T. N. Chen, A. G. Yodh, and C. B. Murray, Proc. Natl. Acad. Sci. (USA) **107**, 22430 (2010).
[22] M. Cavallaro Jr., L. Botto, E. P. Lewandowski, M. Wang, and K. J. Stebe, Proc. Natl. Acad. Sci. (USA) **108**, 20923 (2011).
[23] H. Geerts, M. D. Brabander, R. Nuydens, S. Geuens, M. Moerenmans, J. D. Mey, and P. Hollenbeck, Biophys. J. **52**, 775 (1987).

[24] J. Gelles, B. J. Schnapp, and M. P. Sheetz, Nature (London) **331**, 450 (1988).
[25] M. J. Saxton, Biophys. J. **64**, 1766 (1993).
[26] M. J. Saxton and K. Jacobson, Annu. Rev. Biophys. Biomol. Struct. **26**, 373 (1997).
[27] T. Fujiwara, K. Richie, H. Murakoshi, K. Jacobson, and A. Kusumi, J. Cell Biol. **157**, 1071 (2002).
[28] M. Dahan, S. Lévi, C. Luccardini, P. Rostaing, B. Riveau, and A. Triller, Science **302**, 442 (2003).
[29] J. Suh, M. Dawson, and J. Hanes, Adv. Drug. Del. Rev. **57**, 63 (2005).
[30] D. Weihs, T. G. Mason, and M. A. Teitell, Biophys. J. **91**, 4296 (2006).
[31] K. I. Willig, R. R. Kellner, R. Medda, B. Hein, S. Jakobs, and S. W. Hell, Nat. Meth. **3**, 721 (2006).
[32] K. Ritchie and J. Spector, Biopolymers **87**, 95 (2007).
[33] A. Triller and D. Choquet, Neuron **59**, 359 (2008).
[34] A. Sergé, N. Bertaux, H. Rignault, and D. Marguet, Nat. Meth. **5**, 687 (2008).
[35] K. Jaqaman, D. Loerke, M. Mettlen, H. Kuwata, S. Grinstein, S. L. Schmid, and G. Danuser, Nat. Meth. **5**, 695 (2008).
[36] S. Wieser and G. J. Schütz, Methods **46**, 131 (2008).
[37] T. J. Gould, M. S. Gunewardene, M. V. Gudheti, V. V. Verkhusha, S.-R. Yin, J. A. Gosse, and S. T. Hess, Nat. Meth. **5**, 1027 (2008).
[38] M. J. Saxton, Nat. Meth. **5**, 671 (2008).
[39] D. Wirtz, Annu. Rev. Biophys. **38**, 301 (2009).
[40] D. M. Owen, D. Williamson, C. Rentero, and K. Gaus, Traffic **10**, 962 (2009).
[41] D. Alcor, G. Gouzer, and A. Triller, Eur. J. Neurosci. **30**, 987 (2009).
[42] C. A. Day and A. K. Kenworthy, Biochim. Biophys. Acta **1788**, 245 (2009).
[43] C. Eggeling, C. Ringemann, R. Medda, G. Schwarzmann, K. Sandhoff, S. Polyakova, V. N. Belov, B. Hein, C. von Middendorf, A. Schönle *et al*., Nature (London) **457**, 1159 (2009).
[44] K. Braeckmans, K. Buyens, W. Bouquet, C. Vervaet, P. Joye, F. D. Vos, L. Plawinski, L. Doeuvre, E. Angles-Cano, N. N. Sanders *et al*., Nano Lett. **10**, 4435 (2010).
[45] A. J. García-Sáez and P. Schwille, Biochim. Biophys. Acta **1798**, 766 (2010).
[46] E. Betzig and R. J. Chichester, Science **262**, 1422 (1993).
[47] C. Ribrault, A. Triller, and K. Sekimoto, Phys. Rev. E **75**, 021112 (2007).
[48] H. Fujisaka and M. Inoue, J. Phys. Soc. Jpn. **70**, 2283 (2001).
[49] M. Yoshida, S. Miyazaki, and H. Fujisaka, Phys. Rev. E **74**, 026204 (2006).
[50] H. Touchette, Phys. Rep. **478**, 1 (2009).
[51] H. Nakao, S. Kitada, and A. S. Mikhailov, Phys. Rev. E **74**, 026213 (2006).
[52] K. Ouchi, T. Horita, and T. Yamada, Phys. Rev. E **83**, 046202 (2011).